nature astronomy

Article

https://doi.org/10.1038/s41550-022-01811-y

A fast-rising tidal disruption event from a candidate intermediate-mass black hole

Received: 11 April 2022

Accepted: 20 September 2022

Published online: 10 November 2022

Check for updates

C. R. Angus[1], V. F. Baldassare[2], B. Mockler[3], R. J. Foley[3], E. Ramirez-Ruiz[1,3], S. I. Raimundo[1,4,5], K. D. French[6,7], K. Auchettl[3,8,9], H. Pfister[1,10], C. Gall[1], J. Hjorth[1], M. R. Drout[11,12], K. D. Alexander[13], G. Dimitriadis[3,14], T. Hung[3], D. O. Jones[3], A. Rest[15,16], M. R. Siebert[3], K. Taggart[3], G. Terreran[17,18], S. Tinyanont[3], C. M. Carroll[2], L. DeMarchi[13], N. Earl[6], A. Gagliano[6,7], L. Izzo[1], V. A. Villar[19,20,21], Y. Zenati[15], N. Arendse[1], C. Cold[1], T. J. L. de Boer[22], K. C. Chambers[22], D. A. Coulter[3], N. Khetan[1], C. C. Lin[22], E. A. Magnier[22], C. Rojas-Bravo[3], R. J. Wainscoat[22] & R. Wojtak[1]

Massive black holes (BHs) at the centres of massive galaxies are ubiquitous. The population of BHs within dwarf galaxies, on the other hand, is not yet known. Dwarf galaxies are thought to harbour BHs with proportionally small masses, including intermediate-mass BHs, with masses $10^2 < M_{\mathrm{BH}} < 10^6$ solar masses ($M_{\odot}$). Identification of these systems has historically relied on the detection of light emitted from accreting gaseous disks close to the BHs. Without this light, they are difficult to detect. Tidal disruption events, the luminous flares produced when a star strays close to a BH and is shredded, are a direct way to probe massive BHs. The rise times of these flares theoretically correlate with the BH mass. Here we present AT 2020neh, a fast-rising tidal disruption event candidate, hosted by a dwarf galaxy. AT 2020neh can be described by the tidal disruption of a main sequence star by a $10^{4.7}$–$10^{5.9}$ $M_{\odot}$ BH. We find the observable rate of fast-rising nuclear transients like AT 2020neh to be low, at $\lesssim 2 \times 10^{-8}$ events Mpc^{-3} yr^{-1}. Finding non-accreting BHs in dwarf galaxies is important to determine how prevalent BHs are within these galaxies, and to constrain models of BH formation. AT 2020neh-like events may provide a galaxy-independent method of measuring the masses of intermediate-mass BHs.

In Fig. 1 we present the nuclear transient, AT 2020neh. AT 2020neh was first reported by the Zwicky Transient Facility (ZTF)[1] on 19 June 2020 at right ascension 15 h 21 min 20.07 s and declination +14° 4′ 10.74″ (J2000), and was confirmed with Young Supernova Experiment (YSE) data[2], which showed an initial earlier detection on 17 June 2020. The location of the transient, confirmed in late-time imaging from the Hubble Space Telescope (Fig. 1), is coincident with the nucleus of the galaxy, lying within 0.1″ of the centre. Host-galaxy spectral lines constrain the redshift of the event to $z = 0.062$ (~280 Mpc). AT 2020neh reached peak brightness on 1 July 2020, and was monitored with multi-wavelength follow-up observations for over 400 days from peak in the rest frame (see the Methods for details of the follow-up campaign). The full ultraviolet and optical light curves for AT 2020neh are shown in Extended Data Fig. 1.

We present our spectroscopic follow-up observations of AT 2020neh in Fig. 2. The classification spectrum, obtained using the Nordic Optical Telescope on 25 June 2020, 6 days before maximum light, shows a strong blue continuum with a clearly blended helium II λ4685 and nitrogen III λ4640 emission feature and no traces of hydrogen. This blended emission feature has been observed for several

A full list of affiliations appears at the end of the paper. e-mail: angus@nbi.ku.dk

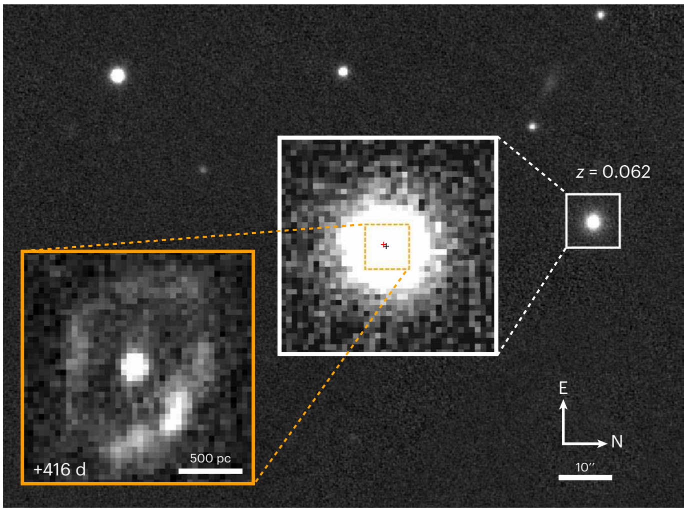

Fig. 1 | The nuclear transient AT 2020neh. The main image shows the environment of AT 2020neh in optical Pan-STARRS1 Survey (PS1) r-band imaging. The dwarf host galaxy of the transient is highlighted. The inset with the white border shows the apparent location of AT 2020neh within its host galaxy in the optical. The host centroid is marked with a black cross and the location of AT 2020neh is marked with a red cross (shown with 1 σ astrometric uncertainties). The location of the transient is coincident with the host nucleus. The inset with the orange border shows deep-UV imaging from the Hubble Space Telescope of AT 2020neh at +416 d. The transient is still clearly detected at the centre of the host, surrounded by a ring of star formation approximately 600 pc from the nucleus.

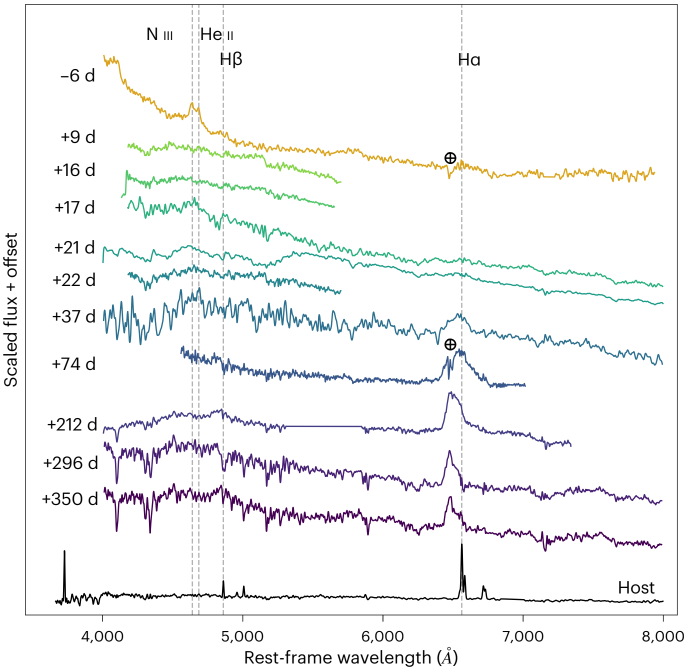

Fig. 2 | The spectroscopic evolution of AT 2020neh. Common TDE emission features (H, He, N) are marked. The strong He II and N III emission seen pre-maximum light disappears after the peak, with Balmer emission appearing at much later epochs and becoming increasingly asymmetric and blueshifted as the TDE evolves. Spectra have been scaled and offset for clarity, with their rest-frame phases indicated. Crossed circles mark telluric features still present within the spectra. The instruments used to obtain these data are listed in Supplementary Table 1.

optical tidal disruption events (TDEs)[3–7], and is attributed to a fluorescence mechanism requiring both a high-energy radiation source and a high gas density[8]. Given the nuclear location of the transient (Fig. 1), we interpret these features under a TDE classification for the transient AT 2020neh. The spectra become featureless after maximum light, evolving to gradually reveal a broad hydrogen, Hα, emission line at +36 d (and later in Hβ too). This Hα emission dominates the late-time spectra of AT 2020neh, exhibiting an asymmetric profile that is blueshifted with respect to the rest frame by ~4,000 km s^{-1} (Table 1). The profile of this emission is consistent with emission lines arising from optically thick outflowing material[9], which has been seen in several other TDEs (for example, refs. [7,10–12]). The lack of elements heavier than hydrogen within the late-time (>200 d) spectra is consistent with a TDE classification, as these elements would only be expected if the event arose from a stellar explosion[13].

Only a dozen TDEs have optical light curves with sufficient data coverage at early times to confidently determine the time taken for the transient to reach maximum light (see ref. [14]). In Fig. 3 we show the distribution of their rise times and luminosities, alongside those of AT 2020neh. The constraining non-detections from frequent YSE monitoring before first detection of the transient and the depth of the YSE imaging result in an exceptionally well-constrained rise time for this event. With information on the evolution of AT 2020neh down to 3% of its maximum light, we measured a rise time from initial detection to g-band peak of only 13.2 ± 1.0 d in the rest frame. This rise time is on average a factor of $2.4^{+3.0}_{-1.5}$ times faster than the median rise time of other TDEs with pre-max light curve coverage. AT 2020neh attained a peak bolometric luminosity of $4.2 \pm 0.1 \times 10^{43}$ erg s^{-1}. Although this luminosity alone is not unprecedented amongst TDEs, when taken into consideration with its short rise time it places AT 2020neh on the periphery of the known nuclear transient luminosity–rise parameter space, being brighter than other confirmed TDEs with short rise times. This unique location places AT 2020neh between TDEs and another class of transients: fast and blue optical transients (FBOTs; for example refs. [15–17]). Despite this similarity in rise time, AT 2020neh shows important differences in both its spectroscopic properties and its photometric evolution from those of FBOTs (Methods), that set it apart from this class. We found that the post-maximum evolution of AT 2020neh was typical of other TDEs, being well described by a power-law decline slope of $\alpha = 1.44 \pm 0.19$. This is consistent with the theoretical −5/3 slope expected from transients powered by fallback accretion[18].

The host galaxy of AT 2020neh, SDSS J152120.07+140410.5, is unusual among the population of TDE host galaxies (Methods). The galaxy is blue in colour and a pre-explosion Sloan Digital Sky Survey (SDSS) spectrum of the host galaxy shows that it is star forming (Extended Data Fig. 2). However, the galaxy also has a high Sérsic index and a high surface density concentration of stellar mass relative to field galaxies. This increases the number of stars capable of being disrupted, which has been seen within other TDE host galaxies[19–21]. When we measured the stellar mass of SDSS J152120.07+140410.5, we found it to be $\log(M_\star/M_\odot) = 9.57 \pm 0.20$. This mass is consistent with the masses of dwarf galaxies, and is about the same as the mass of the Large Magellanic Cloud. Scaling relations between galaxy stellar mass and black hole (BH) mass (derived from more massive galaxy populations; ref. [22]) predict that for such small galaxies, we expect correspondingly low-mass BHs. Direct evidence for the presence of BHs in low-mass galaxies, however, is scarce (see ref. [23]). These systems are typically faint, and the gravitational sphere of influence for low-mass BHs is predicted to be small, making them difficult to resolve in observations of galaxies outside of the Local Group. Thus the occupation fraction of BHs at the low-mass end of the galaxy stellar mass regime remains observationally unconstrained[24]. The detection of AT 2020neh thus indicates the presence of a BH in a dwarf galaxy, from which we could begin to explore the properties of the BH.

Table 1 | Properties of the Hα emission observed in the spectra of AT 2020neh

Phase (d)	Flux($\times10^{-15}$ erg s^{-1})	*Observed Wavelength*, $\lambda_{\rm observed}$(Å)	Velocity offset(km s^{-1})	Equivalent Width(Å)
+37	4.78±0.04	6,528±3	−1,526±137	80±9
+74	16.10±0.08	6,525±10	−1,709±457	105±12
+212	18.65±0.02	6,480±1.0	−3,767±46	129±8
+296	3.02±0.03	6,475.1±1.3	−3,990±65	80±3
+350	3.14±0.04	6,475.2±1.7	−3,990±79	82±4

The unique location of AT 2020neh in Fig. 3 implies a relative scarcity of similar events among the TDE population. Indeed, we estimated the observable rate of fast-rising TDEs like AT 2020neh to be $\lesssim 2\times10^{-8}$ Mpc^{-3} yr^{-1} at $z = 0.27$, the detection limit of the YSE survey (Methods). This is approximately one-twenty-fifth of the 'normal' TDE rate[25]. The relatively low rate of fast TDEs may be explained through the mechanics of the BH–stellar encounter. For low-mass ($<10^6\,M_\odot$) BHs, the event horizon of the BH is much smaller than the tidal radius required to disrupt a star of average mass. Therefore, for the event to be observed as a 'classical TDE', one whose luminosity closely follows the rate at which material falls onto the BH (the fallback rate), a plunging encounter is required. Such an encounter allows the material to circularize quickly enough for the event to be observable[26], as found when modelling AT 2020neh (Methods). Events with shallower, grazing encounters are unlikely to circularize their debris into an accretion disk on timescales shorter than the timescale of peak fallback accretion. This is a consequence of weaker general relativistic effects around smaller BHs. These encounters are thought to produce less-luminous transients with irregular light curves that are unlikely to be observable[27]. We estimated that the peak luminosity of AT 2020neh would exceed the maximum (Eddington) luminosity ($L_{\rm Edd}$) at which the BH can radiate by a factor of ~2–3 for its measured BH mass range[28]. This is in agreement with theoretical predictions, as observable TDEs around lower-mass BHs are also likely to be 'super-Eddington' flares, as a result of their predicted high fallback rates[27].

The properties of the TDE light curve can potentially be used to probe the BH mass[29], which could provide a measurement independent of assumptions about the host galaxy. The rise time of a TDE, Δt, which is the time taken between disruption of the star to peak luminosity of the event, theoretically correlates with the BH mass. This is because the luminosity of the transient is expected to follow the fallback rate of the stellar debris with a relationship $\Delta t \propto M_{\rm BH}{}^{0.5}$(ref. [29]; see Methods for modelling details). When we fitted the multi-band UV–optical light curve of AT 2020neh (Extended Data Fig. 3), we found $\log M_{\rm BH}/M_\odot = 5.5^{+0.4}_{-0.3}$. We note that the physical origins of the early optical emission in TDEs is unknown, so this approach to BH mass estimation may not be applicable to all events. We assessed the reliability of this measurement with two galaxy–BH scaling relationships. The $M_\star$–$M_{\rm BH}$ scaling relation[22] predicts a BH mass of $\log M_{\rm BH}/M_\odot = 5.9 \pm 0.2$ We used a late-time high-resolution spectrum of the TDE to measure the velocity dispersion ($\sigma_\star$) of the host galaxy. We measured $\sigma = 39 \pm 13$ km s^{-1}, which, using an $M_{\rm BH}$–$\sigma_\star$ relation[30], provides a BH mass of $\log M_{\rm BH}/M_\odot = 4.8^{+0.5}_{-0.9}$. These are both consistent with the mass estimated from the rise of the light curve. Our constraints on the mass range of the BH, $4.7 < \log M_{\rm BH}/M_\odot < 5.9$, place it within the domain of intermediate-mass BHs, whose masses span the gap between stellar-mass and supermassive BH populations ($2 \lesssim \log M_{\rm BH}/M_\odot \lesssim 6$), but for which evidence of a firm population has been difficult to obtain[31].

The massive BHs ($M_{\rm BH} \gtrsim 10^9\,M_\odot$) we observe in the hearts of galaxies in the local Universe[32] must originate from less-massive BHs that have grown through mergers or the accretion of surrounding material. How this putative 'seed' population of less-massive BHs forms is unclear. Possible formation mechanisms include hierarchical mergers of stellar-mass BHs[33], core collapse of exceptionally massive stars in the early Universe[34] and the direct collapse of massive gas clouds[35]. Measuring the low-mass ends of the BH mass function and BH–galaxy scaling relationships is important to distinguish between these scenarios, as each model is predicted to influence the slope of these relationships differently[31]. Identifying BHs in dwarf galaxies and measuring their masses is generally difficult[23,36–38] due to their intrinsically low luminosity and smaller gravitational influence. Typically, signatures of BH accretion (an active galactic nucleus (AGN)) are required to reliably confirm the presence of a BH in a dwarf galaxy (for example, refs. [39–42]). However, the majority of BHs are not active. Fast-rising optical TDE candidates such as AT 2020neh may therefore offer an opportunity to find and study non-active BHs in dwarf galaxies.

In Fig. 4 we display the location of AT 2020neh on two commonly used BH–galaxy scaling relations. AT 2020neh is a candidate optical TDE from an intermediate-mass BH in a dwarf galaxy, and its host galaxy is one of only a small number of dwarf galaxies that has a BH mass estimate independent of galaxy scaling relationships. At present, most galaxies in the low-stellar-mass/low-velocity-dispersion regions of BH scaling relations are low-luminosity AGN, and therefore not representative of the quiescent dwarf galaxy population. A handful of X-ray-detected transients in dwarf galaxies have also had a intermediate-mass BH–TDE origin proposed[43–45], for which the BH mass estimates have been derived from galaxy-scaling relationships from fitting of the X-ray spectrum with disk models. AT 2020neh represents a population of optically detected transients whose properties may allow us to explore the low-mass end of BH scaling relations in a complementary way. The relative rate of fast TDEs to normal TDEs implies that other events like AT 2020neh should be more common amongst the TDE population. Early detection of future fast TDEs within deep, high-cadenced datasets, like the early YSE detection of AT 2020neh,

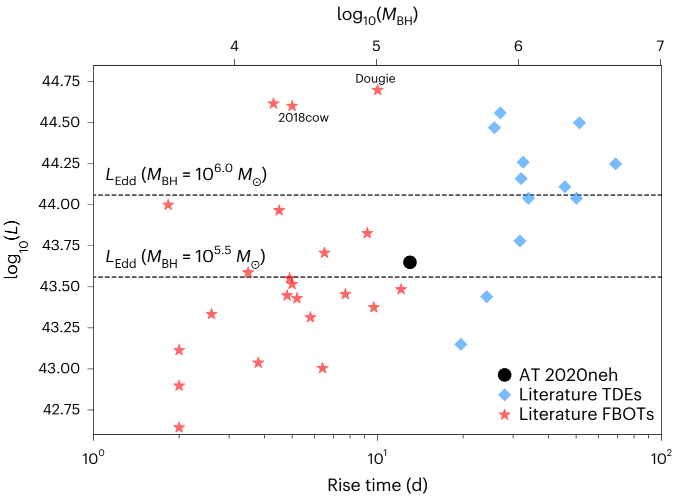

Fig. 3 | The rise–luminosity distribution of TDEs and FBOTs. The measured rise times of TDEs from the literature with pre-peak coverage are shown as a function of their peak luminosities (L). AT 2020neh occupies a unique position within this parameter space (fast for a TDE and brighter than other short-lived TDEs), lying between TDEs and the FBOT population[17]. More energetic FBOT events such as Dougie[15] and AT 2018cow[16] are marked. Using the transient rise time to estimate the BH mass for the TDE events (top x axis), we can see that 'faster rising' AT 2020neh-like events probe the regions of super-Eddington accretion for lower-mass BHs (dashed lines mark the Eddington limits for BHs with $M_{\rm BH} < 10^{6.0}\,M_\odot$ and $M_{\rm BH} < 10^{5.5}\,M_\odot$).

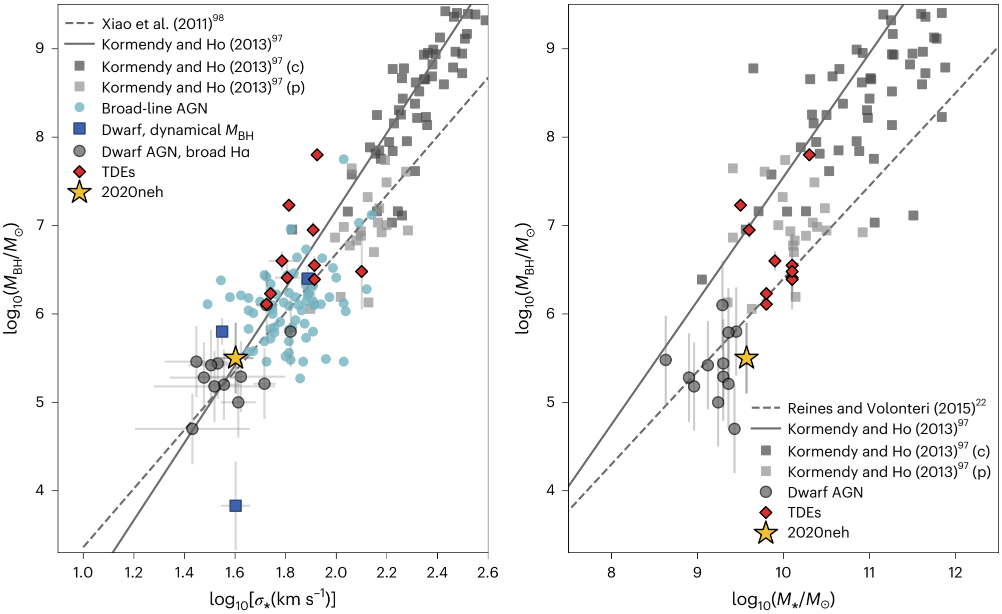

Fig. 4 | BH scaling relations including dwarf galaxies. Left: BH mass versus stellar velocity dispersion for samples of local galaxies. Right: BH mass versus galaxy stellar mass. Compilation samples of galaxies from ref. [97] (classic-bulge and pseudo-bulge galaxies marked as 'c' and 'p' respectively) and broad-line AGN from ref. [98] are shown, alongside dwarf galaxies with dynamical mass measurements 97 and fits to the scaling relationsfrom ref. [22,97,98]. Data points for dwarf AGN are from refs. [36,42]. TDEs with BH mass estimates are from ref. [29]. Measurements are presented with ±1 σ uncertainties. The majority of galaxies with BH mass estimates in the low-stellar-mass/low-velocity-dispersion regime are those derived from the velocity of gas in the broad-line region using the Hα line, which has large uncertainties. AT 2020neh is one of a few BHs with an independent mass estimate in this region.

will generate the samples of events with constraining datasets needed to test the reliability of BH masses estimated from rise-time measurements. The properties of AT 2020neh will form the baseline from which targeted observing strategies can be designed to ensure maximum scientific gain from the discovery of fast TDEs in current and future surveys. We estimate that YSE will observe another 5–6 similar events over its lifetime, each with the necessary light curve data to constrain the rise time.

Methods

Throughout this work we assumed a standard Λ cold dark matter cosmology (where Λ is the cosmological constant) with the Hubble constant $H_0 = 71\ \mathrm{km\ s^{-1}\ Mpc^{-1}}$, the matter density $\Omega_M = 0.27$ and the vacuum energy-density $\Omega_\Lambda = 0.73$.

Data

Optical photometry. The optical photometry of AT 2020neh was obtained by the YSE sky survey[2] with the 1.8 m PS1. PS1 is mounted with a 1.4 gigapixel camera[46] to image the sky in the g, r, i and z filters. The data were downloaded, processed and archived using the image processing pipeline at the University of Hawaii's Institute for Astronomy[47]. Images from the PS1 3π survey were used as references for template subtraction, with each reference image convolved to match the point spread function of the nightly observations, before passing through the Transient Science Server at Queens University Belfast[48] to identify new events. The YSE photometric pipeline is based on PHOTOPIPE[49]. Forced point spread function photometry was performed for each transient, using a flux weighted centroid matching the point spread function at the transient location.

The field in which AT 2020neh is located was monitored by YSE for three months before the first detection of the transient, with non-detections at 18 epochs over this period in which no light from the transient is observed. These data provide strong constraints on the explosion epoch down to limiting magnitudes of typically $m \approx 21.5$ mag in the g, r and i bands and $m \approx 20.5$ mag in the z band. Additional g- and r-band photometry of AT 2020neh was taken from the public ZTF[50,51] data stream, with observational coverage from 19 June 2020 to 4 August 2020 (−12 to +35 d in the rest-frame phase).

Optical spectroscopy. Spectra were obtained using the instruments and observational set-ups listed in Supplementary Table 1. The Andalucia Faint Object Spectrograph and Camera (ALFOSC), Kast and Low Resolution Imaging Spectrometer (LRIS) spectra were reduced using custom-made pipelines and standard routines within IRAF. The Gemini Multi-Object Spectrographs (GMOS) spectra were processed using the Gemini IRAF package. The DEep Imaging Multi-Object Spectrograph (DEIMOS) spectrum was processed with the PypeIt software package[52]. All calibrations and correction procedures were performed after the basic pipeline reduction using custom Python programs. Spectra were corrected for an average Galactic extinction along the line of sight to the transient of $E(B-V) = 0.038$ mag and a total-to-selective extinction ratio $R_V = 3.1$ based on the dust maps of ref. [53]. We used a pre-transient SDSS[54] spectrum of the host galaxy to correct for the host-galaxy contribution to the spectra. We colour-corrected both transient and host-galaxy spectra using the technique of ref. [55] to the available g, r, i and z photometry from PS1 to correct for slit/fibre losses. For the low-resolution ALFOSC and Kast spectra, we convolved this host-galaxy spectrum to the resolution of these instruments before subtraction. For higher-resolution spectra, we created models of the host-galaxy emission lines based on measurements from the SDSS spectrum and subtracted these models from the science spectra. All line measurements were performed using the specutils package in Python (https://specutils.readthedocs.io/en/stable/index.html). We note that several narrow stellar absorption features with widths smaller than the instrumental resolution of the SDSS spectrograph still persisted within our host-galaxy subtracted spectra (a consequence of the low velocity dispersion of the host galaxy; see below).

Swift observations. We requested, and were awarded, target-of-opportunity observations from the Neil Gehrels Swift Gamma-ray Burst Mission (Swift) UltraViolet and Optical Telescope (UVOT) and X-ray Telescope (XRT). AT 2020neh was monitored with Swift over two epochs while the transient was active; from 1 July 2020 to 17 July 2020, and from 5 August 2020 to 6 September 2020 with an approximate 2 d cadence. Final Swift observations were also obtained between 13 January 2021 and 27 January 2021 and averaged to estimate the host-galaxy level for subtraction. To obtain the UVOT photometry, we used the task UVOTSOURCE with source radii of 5.0″ and background radii of 40.0″. The transient was clearly detected with UVOT during the first two epochs. The host-galaxy-subtracted UVOT light curve is presented in Extended Data Fig. 1.

XRT was operated in the photon counting mode for all observations. We reprocessed the data with the task XRTPIPELINE version 0.13.2 using standard filters, screen and recent calibration files. Using a source region centred on the location of AT 2020neh with a radius of 49″ and a 150″ radius source-free-background region centred at 15 h 21 min 4.77 s, +13° 59′ 37.78″, we detected no significant X-ray emission arising from the source. To constrain any X-ray emission, we merged all 37 Swift XRT observations of AT 2020neh using the task XSELECT. We derived a 3 σ upper limit on the 0.3–10.0 keV count rate of 0.002 counts s^{-1}. Assuming an absorbed power-law model with a column density of 2.7×10^{20} cm^{-2} (ref. [56]) and a photon index, $\Gamma = 2.7$ (similar to that of other X-ray bright TDEs; for example, ref. [57]), redshifted to the location of the host galaxy, we found a 3 σ upper limit on the unabsorbed X-ray luminosity of 4.5×10^{41} erg s^{-1}. This faint X-ray luminosity is consistent with other previously observed TDEs[57] and suggests that the source does not harbour a strong AGN component, congruous with the composite location of the host galaxy in the "Baldwin, Phillips & Terlevich" (BPT) diagram (Extended Data Fig. 2).

Radio observations. AT 2020neh was observed twice during its evolution with the Very Large Array under programme VLA/20B-377 (PI: K.D.A.). The first observation was conducted on 30 June 2020 (−1 d from peak in the TDE rest frame) at 15 GHz. The source was not detected with a 3 σ upper limit of 18 μJy. The second observation on 31 December 2020 (+172 d rest frame) at 6 GHz also resulted in a non-detection, with a 3 σ upper limit of 16 μJy. These limits are consistent with a lack of a relativistic jet[58], and further support the conclusion that the host galaxy does not harbour an obvious AGN (see 'Host galaxy properties' below).

Hubble Space Telescope observations. We observed AT 2020neh on 16 September 2021 with the Wide Field Camera 3 on the Hubble Space Telescope (HST) under programme SNAP-16239 (PI: R.J.F.). AT 2020neh was imaged in F225W and F275W for a total exposure time of 780 and 710 s, respectively. Two images were taken in each band to reject cosmic rays. The data were processed through the STScI data reduction pipeline, including basic processing, calibration and drizzling.

AT 2020neh was clearly detected in the HST images at the centre of its host galaxy surrounded by a circumnuclear ring with a projected radius of 0.35–0.7″, corresponding to physical distances of 0.45–0.9 kpc at $z = 0.062$. We performed photometry using the automatic detection and extraction package Source Extractor (SExtractor)[59], applying a surface brightness signal-to-noise cut of two per pixel to include faint surface brightness features and adjusting the extraction parameters to separate the TDE from the star-forming ring. Zero points for each filter were taken from the STScI WFC3 handbook[60]. We measured $m_{\rm F225W} = 22.059 \pm 0.022$ and $m_{\rm F275W} = 21.790 \pm 0.019$.

Transient classification

The photometric properties of AT 2020neh make it exceptional amongst the nuclear transient population, with a fast rise and luminous peak that require careful classification. In particular, it was important to distinguish this event from hydrogen-rich core collapse supernovae (type II supernovae), as the evolutionary timescales and hydrogen spectral features are similar to this class. It was also important to establish whether AT 2020neh could be classified as an FBOT event. Below we present the evidence for a TDE origin for AT 2020neh.

Spectroscopic behaviour. The dominant feature present within the Nordic Optical Telescope (NOT) spectrum taken pre-maximum light is a strong blended He II and N III emission feature around 4,660 Å. This feature was no longer detectable within the first post-max spectrum obtained at +9 d with GMOS. Such short-lived features have been observed within samples of young type II supernovae, where the high-energy UV emission that occurs during shock break-out briefly ionizes any surrounding circumstellar material, recombining to produce strong emission lines (for example ref. [61]; see also Supplementary Fig. 1). Supernovae that exhibit these 'flash ionization' features are typically accompanied by Balmer emission lines, which we did not observe with AT 2020neh at this epoch (all Balmer features observed in the NOT spectrum were consistent with the SDSS spectrum of the host galaxy). Based on the velocities observed for the He II/N III emission (950 ± 160 km s^{-1}), we should have observed any flash ionized Balmer emission present within this early spectrum.

The later spectroscopic evolution of AT 2020neh also did not follow the canonical behaviour of a type II supernova. We only began to observe Hα emission at later epochs (>37 d from peak), when it presented a broad, boxy blueshifted emission profile with no accompanying absorption. Although there is diversity in the Hα features present within type II supernovae spectra[62,63], Hα nominally takes on a P Cygni profile for these events due to the expanding, optically thick material ejected from the progenitor. For AT 2020neh to be a type II supernova, the lack of P Cygni signature in its Hα emission would require either the photosphere to be very small compared with the expanding material, or there to be optically thin material along the line of sight masking the photosphere. The first scenario is rare, seen only in a few type II supernovae at very early times[62]. The second scenario requires the observed Hα emission to be produced via interaction (as for type IIn supernovae), for which we would expect to see very narrow features (~200 km s^{-1}). We did not observe this narrow emission in AT 2020neh. Although blueshifted Balmer features have been observed within some type II supernovae, they typically occur at much smaller velocity shifts (population mean 2,000 km s^{-1}; ref. [64]) compared with the ~4,000 km s^{-1} shift observed within AT 2020neh. Type II supernova blueshifts also evolve with time, disappearing by the nebular phase. The Hα line remained blueshifted until late times, and did not appreciably evolve during the later stages of its evolution. Finally, the late-time (>200 d) spectra of AT 2020neh did not show the forbidden lines [Ca II], [O I] and [Fe II] traditionally observed during the nebular phase in type II supernovae[13,63].

There are few FBOTs with spectroscopic datasets sufficient to determine the typical spectroscopic features of this class. Those that do generally exhibit hot, featureless spectra[15,17,65]. The luminous and local AT 2018cow[16,66] is the only FBOT with sufficient spectroscopic data to make any meaningful comparisons. Post-peak Hα emission has also been observed within this event; however, it is markedly narrower than the Hα seen in AT 2020neh at similar phase[66], even when accounting for the narrower component that was observed at much later epochs (which exhibited velocities of the order of 2,000 km s^{-1}).

Although not typical of optically selected TDEs[25,67], these spectroscopic properties can all be interpreted within a TDE framework. We attributed the blended He II and N III early emission feature to Bowen fluorescence (Supplementary Fig. 1), which has been observed within several TDEs[4,7]. Blueshifted, boxy Balmer emission profiles have also been observed within some TDEs (for example, ref. [11]), and have been shown to result from strongly irradiated, outflowing, optically thick material from the system[9]. The widths of the emission lines observed in AT 2020neh are narrower than those seen in other TDEs[25], but these features are dependent on the viewing angle, and therefore could be a result of a system with low inclination[68]. The lack of nebular phase features is also consistent with a non-supernova origin.

Photometric behaviour. Although the fast rise of AT 2020neh does coincide with the distribution of rise times observed for type II supernovae[69], it is noteably more luminous, with a peak luminosity four times brighter than the upper end of the type II supernova luminosity function[70]. To construct the bolometric light curve of AT 2020neh, we interpolated the available photometry (corrected for foreground extinction) in each band using Gaussian processes, a non-parametric interpolation method that treats all data as though they were drawn from a Gaussian distribution over the possible functions the light curve could take. We implemented this using a Python package[71], interpolating at a daily cadence using a Matern-3/2 kernel. We then fitted the resulting spectral energy distributions at each epoch of the interpolated light curves with a simple black body function. From this constructed bolometric curve, we estimated the peak luminosity to be $4.2 \pm 0.1 \times 10^4$ erg s^{-1}.

In the luminosity–rise time parameter space shown in Fig. 3, AT 2020neh occupies a unique position, being fast and also brighter than other shorter-lived TDEs. These two properties are comparable to those observed within FBOT events, known for their short-lived optical lifetimes and often bright peak luminosities. FBOTs are also frequently characterized by their rapidly cooling photospheres[16,17,72], with some events cooling by >10,000 K in the early stages of their declines[16]. The UV–optical light curve of AT 2020neh exhibited considerable cooling during the first 30 d from peak, with a black body temperature decrease of approximately 9,000 K (Supplementary Fig. 2). Although a cooling photosphere is not associated with many optically discovered TDEs, the majority of which exhibit a constant or even increasing temperature after peak[67], apparent cooling of the photosphere has been observed a few events, for example iPTF16fnl, AT 2019qiz and several TDEs discovered by ZTF[3,12,67,73]. The rate of cooling of AT 2020neh is comparable to these events, which typically display a $\Delta T/\Delta t \gtrsim 5{,}000$ K per 20 d period[12,67,73] (where T is temperature) but much slower than the cooling observed in FBOTs like AT 2018cow (Supplementary Fig. 2). As the exact source of the optical emission in TDEs is unknown, alongside the physical mechanisms that produce it, it is not clear why some TDEs exhibit this cooling behaviour. It has been suggested that it may be linked to optically thick outflows, where cooling of the photosphere occurs when the outflow reaches a characteristic photon trapping radius from which photons are able to escape[12]; however, it is not yet clear whether this scenario is applicable to the majority of cooling cases in TDEs.

From only photometric information, it is difficult to discern FBOTs from TDEs from lower-mass BHs. The physical origins of FBOTs are disputed, but some have had a TDE origin suggested for their production (for example, refs. [15,66]). We used the transient rise times to estimate approximate BH masses for TDEs (shown along the top x axis of Fig. 3), assuming a standard encounter with a solar-mass star. Using this metric, we could see that 'faster rising' AT 2020neh-like events probe the regions of super-Eddington accretion for lower-mass ($M_{BH} < 10^{5.5} M_{\odot}$) BHs.

Astrometric location. The location of AT 2020neh within its host galaxy can also be used to help discriminate between theories for its origin. AT 2020neh is located in SDSS J152120.07+140410.5, a galaxy at a spectroscopic redshift of $z = 0.062024$. We used pre-explosion template PS1/3π images to determine the centroid of the host galaxy, which we found to be at RA = 15 h 21 min 20.087 s, dec = +14° 4′ 10.665″ (with a centroid uncertainty of 0.09″). To determine the location of AT 2020neh in the pre-explosion reference images, we performed astrometry using both YSE PS1 images of the transient close to maximum light in the g, r and i bands, and with acquisition imaging from Gemini from 11 July 2020. In all cases we used routine IRAF tasks to determine the coordinates of cross-matched point sources in both transient and reference images, then mapped and transformed these coordinates to find the transient location in the reference image. We found a mean location of RA = 15 h 21 min 20.094 s, dec = +14° 4′ 10.723″ (±0.12″). We cross-checked this location using the late-time UV imaging from HST. We found the HST location to be RA = 15 h 21 min 20.089 s, dec = +14° 4′ 10.546″ (±0.3″), consistent with our ground-based measurements. The larger uncertainty in the HST measurement is due to a lack of corresponding point sources in the UV image, so we used our ground-based estimates as our final location. The location corresponds to a nuclear separation of 0.13″ (or a physical separation of 0.16 ± 0.15 kpc), consistent with the transient being of nuclear origin (Fig. 1). This separation is also consistent with the range of offsets for radio-detected BHs in dwarf galaxies[38]. The nuclear location of the transient is inconsistent with the distribution of locations and offsets observed within the FBOT population from their apparent host galaxies[17,74], which are not typically associated with the centres of their hosts.

Host-galaxy properties

Spectral properties. We obtained optical spectroscopy of the host of AT 2020neh from SDSS. We measured the emission lines present using standard routines within IRAF and plotted the resulting emission line ratios on a BPT diagram[75], shown in Extended Data Fig. 2. The BPT diagram uses emission line ratios to create theoretical regions used to identify the main excitation mechanisms that produce them[76]; namely star formation, AGN shocks or a composite of the two. The host galaxy of AT 2020neh lies within the star-forming region, close to the composite border.

Pre-explosion variability. Given the proximity of the host galaxy to the composite region of the BPT diagram, we considered the possibility that AT 2020neh may have occurred in an environment with a pre-existing accretion disk (and therefore may be the result of AGN activity). From our early monitoring of the field with YSE (coverage from 24 March 2020 to 17 June 2020 in the g, r and i bands down to $m \approx 21.5$ mag), we found no deviations from the mean of the forced photometry outside of a 1σ range at the transient location over this three-month period. We checked for long-term variability using pre-explosion photometry available from ZTF (coverage from 27 March 2018 to 20 June 2020 in the g and r bands) and from the Catalina Real Time Survey, which monitored the host galaxy from 6 April 2005 to 16 June 2013 in a clear filter. We then used the fitting software QSO FIT[77] to fit the pre-explosion photometry datasets to determine whether the light curves exhibited variability characteristic of an AGN. QSO FIT generates a model light curve by modelling each point given the previous detections and a model co-variance matrix for AGN variability, then assesses how well the best-fit damped random walk model describes the data. Variable AGN typically show a dispersion from a random walk model, σ_{var}, greater than 2 (ref. [42]). We found that the host galaxy of AT 2020neh had low variability ($\sigma_{var} = 0.06$ and 1.19 from ZTF and the Catalina Real Time Survey, respectively) and the "significance that the source is an AGN" as measured by QSO FIT[77] to also be low ($\sigma_{QSO} = 2.02$ and 1.53 from ZTF and the Catalina Real Time Survey, where the AGN would typically have $\sigma_{QSO} > 2$; ref. [42]). It is therefore unlikely that AT 2020neh harbours an active AGN or that the transient is due to AGN activity, in agreement with the host-galaxy location on the BPT diagram.

Spectral energy distribution. To perform spectral energy distribution (SED) fitting of the host galaxy of AT 2020neh, we used archival photometry from the PS1 3π catalogue in the g, r, i, z and y filters, alongside J, H and K measurements from the 2 Micron All Sky Survey[78], W1-3 bands from the Wide-field Infrared Survey Explorer (WISE)[79] and near-UV and far-UV photometry from the Galaxy Evolution Explorer[80]. To account for the systematic uncertainties in the photometry and in the physical models being fitted to the emission, we applied a 10%

error floor to all photometry, with a 30% error floor to the WISE W3 photometry, to account for variations in silicate absorption features around 10 μm (ref. [81]).

We then derived the physical properties of the host galaxy by fitting the collated photometry using the stellar population synthesis models in PROSPECTOR[81], considering wide priors on stellar mass, metallicity and star-formation history. We created a model that included the effects of stellar and nebular emission, metallicity, dust reprocessing and an exponentially declining star-formation history. We sampled the posterior using the Bayesian nested sampling code DYNESTY[82]. The galaxy SED and PROSPECTOR fitting results are shown in Extended Data Fig. 2. The model encapsulated the shape of the host-galaxy SED well. We found a stellar mass $\log\,(M_\star/M_\odot)) = 9.57^{+0.02}_{-0.01}$ and a low star-formation rate of $0.33^{+0.06}_{-0.06} M_\odot\,\mathrm{yr}^{-1}$ and a metallicity of $\log(Z/Z_\odot) = 0.13^{+0.19}_{-0.17}$. To account for the uncertainties introduced from assumptions made within the SED fitting on the galaxy star-formation history and dust attenuation laws, we inflated our uncertainties in the stellar-mass estimate to $\log\,(\Delta M_\star/M_\odot)) = 0.19$, in accordance with the average uncertainty in stellar masses fitted with an exponentially declining star-formation history in PROSPECTOR[83].

Using the derived stellar mass, we could estimate the mass of the central BH using a known scaling relation for low-mass galaxies[22]:

$$\log\left(\frac{M_{\mathrm{BH}}}{M_\odot}\right) = \alpha + \beta \log\left(\frac{M_*}{10^{11} M_\odot}\right) \tag{1}$$

where $\alpha = 7.45 \pm 0.08$ and $\beta = 1.05 \pm 0.11$. Using this scaling relation, we estimated the mass of the BH to be $\log M_{\mathrm{BH}}/M_\odot = 5.95^{+0.20}_{-0.20}$.

Spectral modelling. We used the late-time (+74 d rest frame) spectrum of AT 2020neh taken with the DEIMOS spectrograph on Keck to measure the line-of-sight stellar velocity dispersion of the host galaxy. We used regions of the spectrum that were located away from the TDE line emission at this epoch to measure the stellar velocity dispersion to minimize contamination. The resolution of the DEIMOS spectrum ($R \approx 6{,}000$) is finer than that of the archival SDSS spectrum of the host galaxy, and given that the stellar velocity of dwarf galaxies is expected to be low[42], we chose to use this higher-resolution spectrum, rather than the transient-free SDSS spectrum, to estimate the velocity dispersion. We used the penalized pixel fitting software (pPXF)[84,85] to determine the stellar kinematics of the galaxy. pPXF uses the spectral features in a galaxy spectrum alongside a set of stellar templates to determine the stellar line-of-sight velocity distribution. We used the high-resolution spectral templates from the X-shooter Spectral Library[86], which contains spectra of 628 stars in the UVB arm and 718 stars in the VIS arm at a spectral resolution of $R \approx 10{,}000$. We convolved these spectra with a Gaussian of $\sigma = 2.39$ Å to match them to the lower resolution of our DEIMOS spectrum ($R \approx 6,000$). We focused on two wavelength regions covering the Mg Ib triplet at 5,160–5,190 Å and the Na–D doublet at 5,890, 5,895 Å. We fitted each of these regions separately, using the X-shooter UVB and VIS templates. We fitted regions between 4,700–,550 Å and 5,400–6,200 Å (both rest frame), masking the TDE spectrum outside of these windows, and fitting only for the first two moments of the line-of-sight velocity distribution (V and $\sigma_\star$).

To estimate the uncertainty on the velocity dispersion fitted we used a Monte Carlo bootstrap method[87], where we resampled the one-dimensional spectrum on the basis of the error spectrum, and recalculated the velocity dispersion for 1,000 noise realizations. From the resulting distribution of velocities we took the mean to be the final value, and the uncertainty to be the square root of the variance of the distribution. The best-fitting stellar templates are presented in in Supplementary Fig. 3. We found the independently measured velocity dispersions to be $\sigma_\star = 40 \pm 6$ km s^{-1} and $\sigma_\star = 38 \pm 13$ km s^{-1} fitting the UVB and VIS templates, respectively. Given the low signal-to-noise of the host-galaxy stellar features in the VIS arm, we adopted our UVB measurement for our velocity dispersion estimate of the host galaxy.

From the velocity dispersion, we estimated the central BH mass using using a M_{BH}–$\sigma_\star$ relation[30]:

$$M_{\mathrm{BH}} = 1.4 \times 10^8 M_\odot \left(\frac{\sigma}{200\,\mathrm{km\,s^{-1}}}\right)^{4.72}. \tag{2}$$

From our measured velocity dispersion, we estimated the mass of the BH to be $\log M_{BH}/M_\odot = 4.8^{+0.4}_{-0.2}$.

Stellar surface mass density. We examined the stellar surface mass density, $\Sigma M_\star$ of the host galaxy, which, when considered alongside the velocity dispersion of the host galaxy, has been shown to be higher for TDE host galaxies compared with field galaxies in the local Universe[20], increasing the likelihood of a TDE occurring. The stellar surface mass density of the host galaxy is characterized as:

$$\Sigma M_* = \frac{M_*/M_\odot}{r_{50}^2/\mathrm{kpc}^2} \tag{3}$$

where $M_\star$ is our derived stellar mass and r_{50} is the half-light radius enclosing 50% of the host-galaxy flux. Using SExtractor we determined the 50% flux radius using the pre-explosion template PS1/3π image of the host galaxy in the SDSS r-band, setting a detection limit of 3 σ above the background sky. We measured an r_{50} of 1.75 ± 0.07 kpc, which gives a surface mass density of $\log \Sigma M_* = 9.08$.

Comparison with TDE host galaxies. The host galaxy of AT 2020neh has some similarities to the existing population of TDE hosts, but also has properties that make it unique.

The stellar mass of this galaxy places it towards the lower end of the TDE host-galaxy mass function, joining a small but growing number of optical TDEs in dwarf host galaxies[67]. Although this and other measured properties of the host galaxy of AT 2020neh (star-formation rate and BPT location) are not notable outliers among other optical TDE host galaxies (ref. [21], see also Extended Data Fig. 2), the colour of the host galaxy is very blue ($u - r = 1.7$), suggestive of ongoing star formation. This is different to previous TDEs, whose higher-mass host galaxies typically have low star-formation rates or are post-starburst systems[21,88], and increases the possibility of contamination by type II supernovae. However, the host galaxy also possesses a relatively high Sérsic index ($n = 3.2$) and stellar surface mass density compared with SDSS field galaxies. High Sérsic indices have been observed in other TDE hosts[20,88]. These over-densities of stars close to the galaxy nuclei are thought to enhance the TDE rate as they increase the number of stars capable of being disrupted[21]. It may be that this is necessary for the production of a TDE within low-mass star-forming host galaxies.

Light curve modelling

The rate of fallback of the stellar debris from the disrupted star onto the central BH and the peak timescale of the resultant TDE emission are sensitive to the mass of the disrupting BH[27,29,89]. Assuming the emission from the TDE is 'prompt' (that is, follows the fallback rate of material)[27], the light curve can in principle be used to measure the mass of the disrupting BH.

We fitted the multi-band light curve of AT 2020neh using the Modular Open Source Fitter for Transients (MOSFiT) light curve fitting code[90]. The MOSFiT TDE model uses FLASH hydrodynamic simulations of TDEs[91] to calculate the fallback rate of debris for a given TDE set-up (that is, BH mass, stellar mass and impact parameter). Assuming a black body SED, which has been shown to be an excellent approximation of TDE UV and optical emission[6], this is then converted into a bolometric luminosity and parsed through reprocessing and viscosity transformation functions to generate multi-band light curves. Finally, MOSFiT uses a Markov chain Monte Carlo to fit the model light curves to the data. Full details of this model are presented in ref. [29]. When fitting, we did not implement the default Eddington luminosity limit in the TDE model or limit the photospheric size of the transient. Most notably, we were able to place firm constraints on the time of first fallback due to our early YSE photometric limits and detection.

We present our light curve fits from all Markov chain Monte Carlo walkers in Extended Data Fig. 3. We extracted the posterior distributions for the key model parameters from MOSFiT, and found that AT 2020neh is best described by models invoking a star of mass $M_\star = 1.3^{+4.9}_{-1.0}\,M_\odot$, and impact parameter of $\beta = 1.5^{+0.4}_{-0.9}$ (consistent with near full disruption for the best-fit stellar mass) and a BH with $\log M_{\rm BH}/M_\odot = 5.5^{+0.4}_{-0.3}$. The BH mass was consistent with our previous estimates from the host-galaxy properties. We note that the mass of the star was somewhat degenerate with the efficiency parameter in this model[29]. To account for this, systematic uncertainties in the stellar mass (σ_{M_*}) and in the efficiency of converting infalling material into radiation (σ_ϵ), of $\sigma_{M_*} = 0.66$ and $\sigma_\epsilon = 0.68$ were included in our error budget[29]. The strong N abundance observed in the early spectrum of AT 2020neh without accompanying H could suggest a more evolved or stripped progenitor star, although high N abundances have been seen in other TDEs whose inferred stellar masses are consistent with the MOSFiT stellar mass for AT 2020neh[92].

The MOSFiT BH mass is in good agreement with the BH masses inferred from two host-galaxy measurements, increasing confidence in AT 2020neh being produced by an intermediate-mass BH candidate. However, there is still considerable debate around the physical origin of the early optical and UV emission from TDEs, and it is uncertain how well they can be used as an independent way of measuring BH mass. This is needs to be carefully considered when using TDE-inferred BH masses to constrain BH–galaxy scaling relationships.

Although the BH masses inferred from light curve modelling have large inherent uncertainties due to the assumptions made within the model (MOSFiT BH masses have a 0.2 dex systematic error), they are not always in agreement with masses derived via other methods[29]. For instance, some studies have found no correlation between TDE rise time and host-galaxy mass[6,67], which would be expected if the rise time follows the fallback timescale of material onto the BH. In particular, optical TDEs from other low-mass host galaxies have been found to have generally higher MOSFiT BH masses than those inferred from the host-galaxy mass[67]. However, alternative studies have found a moderate scaling between MOSFiT BH masses and the mass of the host-galaxy bulge[93,94]. The discrepancy in BH mass estimates from TDE rise times may be due to the physical origin of the early optical/UV emission. If, rather than following the fallback of material, the rise time of a TDE were actually tracing the radiative diffusion timescale for photons to escape the shock-heated stellar debris, or if the photons were trapped by outflowing material, this would naturally lengthen the time taken to rise to peak[6,14].

It is unclear which, if any, of the proposed physical mechanisms is prevalent in the production of early optical TDE emission. Although there is no firm consensus as to their utility for measuring BH masses, there is tentative evidence to suggest that they could be harnessed for this purpose, once a clearer understanding of their emission is achieved. Larger samples of well-observed TDEs across a range of galaxy masses are required to test this.

Rate estimations and predictions

To estimate the local rate of TDEs with timescales and luminosities comparable to AT 2020neh we assumed the following. Over 24 months of YSE operations we observed only one AT 2020neh-like event, monitoring fields for approximately 6 months each. This equates to one event per year within the YSE observational volume. At the time of writing, the observational footprint of YSE is 750 deg^2 of the northern hemisphere. We performed a volumetric correction to account for the maximum volume over which AT 2020neh could have been detected within the YSE survey ($V_{\rm max}$). Under the current YSE observational strategy[2], we assumed that a fast TDE may rise by 0.2 magnitudes before initial detection. This gave us a maximum redshift of $z = 0.27$, which produced a volume of ~23×10^6 Mpc^3. This provided an approximate observational rate of fast TDEs of $\lesssim 2 \times 10^{-8}$ Mpc^{-3} yr^{-1} at $z = 0.27$.

For comparisons with the normal TDE rate, we took the average per-galaxy TDE rate measurement from ref. [25] for galaxies in the mass range $9.5 < \log \frac{M_*}{M_\odot} < 10.5$and integrated this over the number of galaxies within our $V_{\rm max}$ volume using the redshift-dependent galaxy-mass functions of ref. [95], producing an average rate of ~$10^{-6.3}$ Mpc^{-3} yr^{-1} at $z = 0.27$. We emphasize that this is a conservative estimate as both stochastic effects from measuring rates on the basis of a single object and small observing gaps that lower the YSE detection efficiency for fast transients could lower the estimated rate.

The discovery and functionality of future fast TDE events will heavily depend upon the observing strategies of the surveys they are discovered in. Provided a survey has sufficient depth, future fast TDEs may be detected at any phase of their evolution. However, the utility of AT 2020neh as a probe of the quiescent BH population lies in its early detection to constrain the rise time for BH mass estimates. The cadence of the discovery survey will therefore have the strongest impact on the usefulness of future fast TDEs. High-cadenced deep surveys such as YSE will reliably identify fast TDEs in their infancy. With the planned doubling of the YSE footprint during 2022, based on our earlier rate estimate, we predict that YSE will identify an additional 5–6 events over the remaining 3 years of survey operations.

Data availability

All photometric data are available in Supplementary Table 2 and the spectra of AT 2020neh will be made publicly available to the community via WISeREP[96] (https://www.wiserep.org/object/15046).

Code availability

Code used for LRIS and Kast spectra can be accessed here https://github.com/msiebert1/UCSC_spectral_pipeline. Codes used for the reduction of ALFOSC data and spectral calibration routines, alongside those used for the interpolation and fitting of the photometric data canbe accessed here https://github.com/crangus/.

References

1. Masci, F. J. et al. The Zwicky Transient Facility: data processing, products, and archive. *Publ. Astron. Soc. Pac.* **131**, 018003 (2019).
2. Jones, D. O. et al. The Young Supernova Experiment: survey goals, overview, and operations. *Astrophys. J.* **908**, 143 (2021).
3. Blagorodnova, N. et al. The broad absorption line tidal disruption event iPTF15af: optical and ultraviolet evolution. *Astrophys. J.* **873**, 92 (2019).
4. Leloudas, G. et al. The spectral evolution of AT 2018dyb and the presence of metal lines in tidal disruption events. *Astrophys. J.* **887**, 218 (2019).
5. Holoien, T. W. S. et al. The rise and fall of ASASSN-18pg: following a TDE from early to late times. *Astrophys. J.* **898**, 161 (2020).
6. van Velzen, S. et al. Seventeen tidal disruption events from the first half of ZTF survey observations: entering a new era of population studies. *Astrophys. J.* **908**, 4 (2021).
7. Charalampopoulos, P. et al. A detailed spectroscopic study of tidal disruption events. *Astron. Astrophys.* **659**, A34 (2022).
8. Bowen, I. S. The excitation of the permitted O III nebular lines. *Publ. Astron. Soc. Pac.* **46**, 146 (1934).
9. Roth, N. & Kasen, D. What sets the line profiles in tidal disruption events? *Astrophys. J.* **855**, 54 (2018).
10. Blanchard, P. K. et al. PS16dtm: a tidal disruption event in a narrow-line Seyfert 1 galaxy. *Astrophys. J.* **843**, 106 (2017).
11. Hung, T. et al. Discovery of highly blueshifted broad Balmer and metastable helium absorption lines in a tidal disruption event. *Astrophys. J.* **879**, 119 (2019).

12. Nicholl, M. et al. An outflow powers the optical rise of the nearby, fast-evolving tidal disruption event AT2019qiz. *Mon. Not. R. Astron. Soc.* **499**, 482–504 (2020).
13. Jerkstrand, A. in *The Handbook of Supernovae* (eds Alsabti, A. W. & Murdin P.) 795 (Springer, 2017).
14. Gezari, S. Tidal disruption events. *Annu. Rev. Astron. Astrophys.* **59**, 21–58 (2021).
15. Vinkó, J. et al. A luminous, fast rising UV-transient discovered by ROTSE: a tidal disruption event? *Astrophys. J.* **798**, 12 (2015).
16. Prentice, S. J. et al. The Cow: discovery of a luminous, hot, and rapidly evolving transient. *Astrophys. J. Lett.* **865**, L3 (2018).
17. Pursiainen, M. et al. Rapidly evolving transients in the Dark Energy Survey. *Mon. Not. R. Astron. Soc.* **481**, 894–917 (2018).
18. Rees, M. J. Tidal disruption of stars by black holes of 10^6–10^8 solar masses in nearby galaxies. *Nature* **333**, 523–528 (1988).
19. Law-Smith, J., Ramirez-Ruiz, E., Ellison, S. L. & Foley, R. J. Tidal disruption event host galaxies in the context of the local galaxy population. *Astrophys. J.* **850**, 22 (2017).
20. Graur, O. et al. A dependence of the tidal disruption event rate on global stellar surface mass density and stellar velocity dispersion. *Astrophys. J.* **853**, 39 (2018).
21. French, K. D., Wevers, T., Law-Smith, J., Graur, O. & Zabludoff, A. I. The host galaxies of tidal disruption events. *Space Sci. Rev.* **216**, 32 (2020).
22. Reines, A. E. & Volonteri, M. Relations between central black hole mass and total galaxy stellar mass in the local Universe. *Astrophys. J.* **813**, 82 (2015).
23. Reines, A. E. & Comastri, A. Observational signatures of high-redshift quasars and local relics of black hole seeds. *Publ. Astron. Soc. Aust.* **33**, e054 (2016).
24. Miller, B. P. et al. X-ray constraints on the local supermassive black hole occupation fraction. *Astrophys. J.* **799**, 98 (2015).
25. van Velzen, S., Holoien, T. W. S., Onori, F., Hung, T. & Arcavi, I. Optical-ultraviolet tidal disruption events. *Space Sci. Rev.* **216**, 124 (2020).
26. Guillochon, J., Manukian, H. & Ramirez-Ruiz, E. PS1-10jh: the disruption of a main-sequence star of near-solar composition. *Astrophys. J.* **783**, 23 (2014).
27. Guillochon, J. & Ramirez-Ruiz, E. A dark year for tidal disruption events. *Astrophys. J.* **809**, 166 (2015).
28. Dai, L., McKinney, J. C., Roth, N., Ramirez-Ruiz, E. & Miller, M. C. A unified model for tidal disruption events. *Astrophys. J. Lett.* **859**, L20 (2018).
29. Mockler, B., Guillochon, J. & Ramirez-Ruiz, E. Weighing black holes using tidal disruption events. *Astrophys. J.* **872**, 151 (2019).
30. Merritt, D. & Ferrarese, L. Black hole demographics from the $\mathrm{M}_{\mathrm{ffl}}$-$\sigma$ relation. *Mon. Not. R. Astron. Soc.* **320**, L30–L34 (2001).
31. Greene, J. E., Strader, J. & Ho, L. C. Intermediate-mass black holes. *Annu. Rev. Astron. Astrophys.* **58**, 257–312 (2020).
32. Magorrian, J. et al. The demography of massive dark objects in galaxy centers. *Astron. J.* **115**, 2285–2305 (1998).
33. Giersz, M., Leigh, N., Hypki, A., Lützgendorf, N. & Askar, A. MOCCA code for star cluster simulations - IV. A new scenario for intermediate mass black hole formation in globular clusters. *Mon. Not. R. Astron. Soc.* **454**, 3150–3165 (2015).
34. Schneider, R., Ferrara, A., Natarajan, P. & Omukai, K. First stars, very massive black holes, and metals. *Astrophys. J.* **571**, 30–39 (2002).
35. Loeb, A. & Rasio, F. A. Collapse of primordial gas clouds and the formation of quasar black holes. *Astrophys. J.* **432**, 52 (1994).
36. Baldassare, V. F., Reines, A. E., Gallo, E. & Greene, J. E. X-ray and ultraviolet properties of agns in nearby dwarf galaxies. *Astrophys. J.* **836**, 20 (2017).
37. Baldassare, V. F., Geha, M. & Greene, J. Identifying AGNs in low-mass galaxies via long-term optical variability. *Astrophys. J.* **868**, 152 (2018).
38. Reines, A. E., Condon, J. J., Darling, J. & Greene, J. E. A new sample of (wandering) massive black holes in dwarf galaxies from high-resolution radio observations. *Astrophys. J.* **888**, 36 (2020).
39. Kunth, D., Sargent, W. L. W. & Bothun, G. D. A dwarf galaxy with Seyfert characteristics. *Astron. J.* **93**, 29 (1987).
40. Filippenko, A. V. & Sargent, W. L. W. Discovery of an extremely low luminosity Seyfert 1 nucleus in the dwarf galaxy NGC 4395. *Astrophys. J. Lett.* **342**, L11 (1989).
41. Baldassare, V. F., Reines, A. E., Gallo, E. & Greene, J. E. A ~50,000 $M_{\odot}$ solar mass black hole in the nucleus of RGG 118. *Astrophys. J. Lett.* **809**, L14 (2015).
42. Baldassare, V. F., Dickey, C., Geha, M. & Reines, A. E. Populating the low-mass end of the M_{BH}-σ_* relation. *Astrophys. J. Lett.* **898**, L3 (2020).
43. Donato, D. et al. A tidal disruption event in a nearby galaxy hosting an intermediate mass black hole. *Astrophys. J.* **781**, 59 (2014).
44. Lin, D. et al. A luminous X-ray outburst from an intermediate-mass black hole in an off-centre star cluster. *Nat. Astron.* **2**, 656–661 (2018).
45. He, J. S. et al. Long-term X-ray evolution of SDSS J134244.4+053056.1. A more than 18 year-old, long-lived IMBH-TDE candidate. *Astron. Astrophys.* **652**, A15 (2021).
46. Kaiser, N. et al. Pan-STARRS: A Large Synoptic Survey Telescope Array. In *Survey and Other Telescope Technologies and Discoveries* SPIE Conference Series Vol. 4836 (eds Tyson, J. A. & Wolff, S.) 154–164 (SPIE, 2002).
47. Magnier, E. A. et al. The Pan-STARRS data-processing system. *Astrophys. J. Suppl. Ser.* **251**, 3 (2020).
48. Smith, K. W. et al. Design and operation of the ATLAS transient science server. *Publ. Astron. Soc. Pac.* **132**, 085002 (2020).
49. Rest, A. et al. Testing LMC microlensing scenarios: the discrimination power of the SuperMACHO microlensing survey. *Astrophys. J.* **634**, 1103–1115 (2005).
50. Bellm, E. C. et al. The Zwicky Transient Facility: system overview, performance, and first results. *Publ. Astron. Soc. Pac.* **131**, 018002 (2019).
51. Graham, M. J. et al. The Zwicky Transient Facility: science objectives. *Publ. Astron. Soc. Pac.* **131**, 078001 (2019).
52. Prochaska, J. et al. PypeIt: the Python spectroscopic data reduction pipeline. *J. Open Source Softw.* **5**, 2308 (2020).
53. Schlafly, E. F. & Finkbeiner, D. P. Measuring reddening with Sloan Digital Sky Survey stellar spectra and recalibrating SFD. *Astrophys. J.* **737**, 103 (2011).
54. Aihara, H. et al. The eighth data release of the Sloan Digital Sky Survey: first data from SDSS-III. *Astrophys. J. Suppl. Ser.* **193**, 29 (2011).
55. Hsiao, E. Y. et al. K-corrections and spectral templates of type Ia supernovae. *Astrophys. J.* **663**, 1187–1200 (2007).
56. HI4PI Collaborationet al. HI4PI: A full-sky H I survey based on EBHIS and GASS. *Astron. Astrophys.* **594**, A116 (2016).
57. Auchettl, K., Guillochon, J. & Ramirez-Ruiz, E. New physical insights about tidal disruption events from a comprehensive observational inventory at X-ray wavelengths. *Astrophys. J.* **838**, 149 (2017).
58. Alexander, K. D., van Velzen, S., Horesh, A. & Zauderer, B. A. Radio properties of tidal disruption events. *Space Sci. Rev.* **216**, 81 (2020).
59. Bertin, E. & Arnouts, S. SExtractor: software for source extraction. *Astron. Astrophys. Suppl. Ser.* **117**, 393–404 (1996).
60. Dressel, L. WFC3 Instrument Handbook for Cycle 29. *Baltimore: STScI.* **13**, 343 (2021).

61. Khazov, D. et al. Flash spectroscopy: emission lines from the ionized circumstellar material around <10-day-old type II supernovae. *Astrophys. J.* **818**, 3 (2016).
62. Gutiérrez, C. P. et al. H_α spectral diversity of type II supernovae: correlations with photometric properties. *Astrophys. J. Lett.* **786**, L15 (2014).
63. Gutiérrez, C. P. et al. Type II supernova spectral diversity. I. Observations, sample characterization, and spectral line evolution. *Astrophys. J.* **850**, 89 (2017).
64. Anderson, J. P. et al. Analysis of blueshifted emission peaks in type II supernovae. *Mon. Not. R. Astron. Soc.* **441**, 671–680 (2014).
65. Drout, M. R. et al. Rapidly evolving and luminous transients from Pan-STARRS1. *Astrophys. J.* **794**, 23 (2014).
66. Perley, D. A. et al. The fast, luminous ultraviolet transient AT2018cow: extreme supernova, or disruption of a star by an intermediate-mass black hole? *Mon. Not. R. Astron. Soc.* **484**, 1031–1049 (2019).
67. Hammerstein, E. et al. The final season reimagined: 30 tidal disruption events from the ZTF-I Survey. Preprint at https://arxiv.org/abs/2203.01461 (2022).
68. Parkinson, E. J. et al. Optical line spectra of tidal disruption events from reprocessing in optically thick outflows. *Mon. Not. R. Astron. Soc.* **510**, 5426–5443 (2022).
69. Gonzalez-Gaitan, S. et al. The rise-time of type II supernovae. *Mon. Not. R. Astron. Soc.* **451**, 2212–2229 (2015).
70. Patat, F., Barbon, R., Cappellaro, E. & Turatto, M. Light curves of type II supernovae. II. The analysis. *Astron. Astrophys.* **282**, 731–741 (1994).
71. Ambikasaran, S., Foreman-Mackey, D., Greengard, L., Hogg, D. W. & O'Neil, M. Fast direct methods for Gaussian processes. *IEEE Trans. Pattern Anal. Mach. Intell.* **38**, 252 (2015).
72. Ho, A. Y. Q. et al. The Koala: a fast blue optical transient with luminous radio emission from a starburst dwarf galaxy at z = 0.27. *Astrophys. J.* **895**, 49 (2020).
73. Hinkle, J. T. et al. The curious case of ASASSN-20hx: a slowly-evolving, UV and X-ray luminous, ambiguous nuclear transient. *Astrophys. J.* **930**, 12 (2022).
74. Wiseman, P. et al. The host galaxies of 106 rapidly evolving transients discovered by the Dark Energy Survey. *Mon. Not. R. Astron. Soc.* **498**, 2575–2593 (2020).
75. Baldwin, J. A., Phillips, M. M. & Terlevich, R. Classification parameters for the emission-line spectra of extragalactic objects. *Publ. Astron. Soc. Pac.* **93**, 5–19 (1981).
76. Kewley, L. J., Groves, B., Kauffmann, G. & Heckman, T. The host galaxies and classification of active galactic nuclei. *Mon. Not. R. Astron. Soc.* **372**, 961–976 (2006).
77. Butler, N. R. & Bloom, J. S. Optimal time-series selection of quasars. *Astron. J.* **141**, 93 (2011).
78. Skrutskie, M. F. et al. The Two Micron All Sky Survey (2MASS). *Astron. J.* **131**, 1163–1183 (2006).
79. Wright, E. L. et al. The Wide-field Infrared Survey Explorer (WISE): mission description and initial on-orbit performance. *Astron. J.* **140**, 1868–1881 (2010).
80. Martin, D. C. et al. The Galaxy Evolution Explorer: a space ultraviolet survey mission. *Astrophys. J. Lett.* **619**, L1–L6 (2005).
81. Leja, J., Johnson, B. D., Conroy, C., van Dokkum, P. G. & Byler, N. Deriving physical properties from broadband photometry with Prospector: description of the model and a demonstration of its accuracy using 129 galaxies in the local universe. *Astrophys. J.* **837**, 170 (2017).
82. Speagle, J. S. DYNESTY: a dynamic nested sampling package for estimating Bayesian posteriors and evidences. *Mon. Not. R. Astron. Soc.* **493**, 3132–3158 (2020).
83. Lower, S. et al. How well can we measure the stellar mass of a galaxy: the impact of the assumed star formation history model in SED fitting. *Astrophys. J.* **904**, 33 (2020).
84. Cappellari, M. & Emsellem, E. Parametric recovery of line-of-sight velocity distributions from absorption-line spectra of galaxies via penalized likelihood. *Publ. Astron. Soc. Pac.* **116**, 138–147 (2004).
85. Cappellari, M. Improving the full spectrum fitting method: accurate convolution with Gauss-Hermite functions. *Mon. Not. R. Astron. Soc.* **466**, 798–811 (2017).
86. Gonneau, A. et al. The X-shooter Spectral Library (XSL): data release 2. *Astron. Astrophys.* **634**, A133 (2020).
87. Geha, M. et al. The least-luminous galaxy: spectroscopy of the Milky Way satellite Segue 1. *Astrophys. J.* **692**, 1464–1475 (2009).
88. Hammerstein, E. et al. Tidal disruption event hosts are green and centrally concentrated: signatures of a post-merger system. *Astrophys. J. Lett.* **908**, L20 (2021).
89. Lodato, G. & Natarajan, P. The mass function of high-redshift seed black holes. *Mon. Not. R. Astron. Soc.* **377**, L64–L68 (2007).
90. Guillochon, J. et al. MOSFiT: modular open source fitter for transients. *Astrophys. J. Suppl.* **236**, 6 (2018).
91. Guillochon, J. & Ramirez-Ruiz, E. Hydrodynamical simulations to determine the feeding rate of black holes by the tidal disruption of stars: the importance of the impact parameter and stellar structure. *Astrophys. J.* **767**, 25 (2013).
92. Mockler, B. et al. Constraints on the preferential disruption of moderately massive stars by supermassive black holes. *Astrophys. J.* **924**, 70 (2022).
93. Nicholl, M. Systematic light curve modelling of TDEs: statistical differences between the spectroscopic classes. *Mon. Not. R. Astron. Soc.* **515**, 5604–5616 (2022).
94. Ramsden, P., Lanning, D., Nicholl, M. & McGee, S. L. The bulge masses of TDE host galaxies and their scaling with black hole mass. *Mon. Not. R. Astron. Soc.* **515**, 1146–1157 (2022).
95. McLeod, D. J. et al. The evolution of the galaxy stellar-mass function over the last 12 billion years from a combination of ground-based and HST surveys. *Mon. Not. R. Astron. Soc.* **503**, 4413–4435 (2021).
96. Yaron, O. & Gal-Yam, A. WISeREP—an interactive supernova data repository. *Publ. Astron. Soc. Pac.* **124**, 668 (2012).
97. Kormendy, J. & Ho, L. C. Coevolution (or not) of supermassive black holes and host galaxies. *Annu. Rev. Astron. Astrophys.* **51**, 511–653 (2013).
98. Xiao, T. et al. Exploring the low-mass end of the M_{BH}-σ_* relation with active galaxies. *Astrophys. J.* **739**, 28 (2011).

Acknowledgements

We thank M. Pursiainen for insightful discussions regarding the spectroscopic evolution of this event, and M. Briday for useful instructions regarding the use of PROSPECTOR. C.R.A., J.H., K.A., L.I., C.C., N.K. and R.W. were supported by VILLUM FONDEN Investigator grant (project number 16599). C.R.A., C.G. and L.I. were supported by a VILLUM FONDEN Young Investigator Grant (project number 25501). B.M. acknowledges support from the AAUW Dissertation Fellowship under Swift grant number 80NSSC21K1409. R.J.F., T.H., M.R.S., K.T., S.T. and C.R.-B. were supported in part by NASA grant number 80NSSC20K0953, NSF grant number AST–1815935, the Gordon & Betty Moore Foundation, the Heising-Simons Foundation, and by a fellowship from the David and Lucile Packard Foundation to R.J.F. E.R.-R. acknowledges support from the Heising-Simons Foundation, Nasa Swift and NICER and NSF (grant numbers AST-1911206 and AST-1852393). S.I.R. has received funding from the European Union's Horizon 2020 research and innovation programme under the Marie Sklodowska-Curie grant agreement number 891744. Parts of this research were supported by the Australian Research Council Centre of Excellence for All Sky Astrophysics in 3 Dimensions (ASTRO 3D), through project number CE170100013 and the Australian Research Council Centre of Excellence for Gravitational Wave Discovery (OzGrav) through project number CE170100004. H.P. acknowledges support from the Danish National Research Foundation (grant number DNRF132) and the Hong Kong government (GRF grant numbers HKU27305119 and HKU17304821). M.R.D acknowledges support from the NSERC through grant number RGPIN-2019-06186, the Canada Research Chairs Program, the Canadian Institute for Advanced Research (CIFAR) and the Dunlap Institute at the University of Toronto. D.O.J. is supported by NASA through the NASA Hubble Fellowship grant number HF2-51462.001 awarded by the Space Telescope Science Institute, which is operated by the Association of Universities for Research in Astronomy, Inc., for NASA, under contract number NAS 5-26555. M.R.S. is supported by the National Science Foundation Graduate Research Fellowship Program under grant number. 1842400. D.A.C. acknowledges support from the National Science Foundation Graduate Research Fellowship under grant number DGE1339067. A.G. is supported by the National Science Foundation Graduate Research Fellowship Program under grant number DGE-1746047. A.G. also acknowledges funding from the Center for Astrophysical Surveys Fellowship at UIUC/NCSA and the Illinois Distinguished Fellowship. Some of the data presented herein were obtained at the W. M. Keck Observatory, which is operated as a scientific partnership among the California Institute of Technology, the University of California and NASA. The Observatory was made possible by the generous financial support of the W. M. Keck Foundation. We wish to recognize and acknowledge the very important cultural role and reverence that the summit of Maunakea has always had within the indigenous Hawaiian community. We are most fortunate to have the opportunity to conduct observations from this mountain. Based on observations made with the Nordic Optical Telescope, owned in collaboration by the University of Turku and Aarhus University, and operated jointly by Aarhus University, the University of Turku and the University of Oslo, representing Denmark, Finland and Norway, the University of Iceland and Stockholm University at the Observatorio del Roque de los Muchachos, La Palma, Spain, of the Instituto de Astrofisica de Canarias. Observations were carried out under programme P61-022. A major upgrade of the Kast spectrograph on the Shane 3 m telescope at Lick Observatory was made possible through generous gifts from the Heising-Simons Foundation as well as W. Kast and M. Kast. Research at Lick Observatory is partially supported by a generous gift from Google. This research is based on observations made with the NASA/ESA Hubble Space Telescope obtained from the Space Telescope Science Institute, which is operated by the Association of Universities for Research in Astronomy, Inc., under NASA contract number NAS 5–26555. These observations are associated with programme SNAP-16239. We acknowledge the use of public data from the Swift data archive. Based on observations obtained at the international Gemini Observatory (programme numberGN-2020A-DD-111), a programme of NSF's NOIRLab, which is managed by the Association of Universities for Research in Astronomy (AURA) under a cooperative agreement with the National Science Foundation on behalf of the Gemini Observatory partnership: the National Science Foundation (United States), the National Research Council (Canada), the Agencia Nacional de Investigación y Desarrollo (Chile), the Ministerio de Ciencia, Tecnología e Innovación (Argentina), the Ministério da Ciência, Tecnologia, Inovações e Comunicações (Brazil) and the Korea Astronomy and Space Science Institute (Republic of Korea). We thank the Director for supporting this programme. Based in part on observations obtained with the Samuel Oschin 48-inch Telescope at the Palomar Observatory as part of the Zwicky Transient Facility project. ZTF is supported by the NSF under grant number AST-1440341 and a collaboration including Caltech, IPAC, the Weizmann Institute for Science, the Oskar Klein Center at Stockholm University, the University of Maryland, the University of Washington, Deutsches Elektronen-Synchrotron and Humboldt University, Los Alamos National Laboratories, the TANGO Consortium of Taiwan, the University of Wisconsin at Milwaukee and the Lawrence Berkeley National Laboratory. Operations are conducted by the Caltech Optical Observatories (COO), the Infrared Processing and Analysis Center (IPAC) and the University of Washington (UW). The Pan-STARRS1 Surveys (PS1) and the PS1 public science archive have been made possible through contributions by the Institute for Astronomy, the University of Hawaii, the Pan-STARRS Project Office, the Max Planck Society and its participating institutes, the Max Planck Institute for Astronomy, Heidelberg, and the Max Planck Institute for Extraterrestrial Physics, Garching, The Johns Hopkins University, Durham University, the University of Edinburgh, the Queen's University Belfast, the Harvard-Smithsonian Center for Astrophysics, the Las Cumbres Observatory Global Telescope Network Incorporated, the National Central University of Taiwan, STScI, NASA under grant number NNX08AR22G issued through the Planetary Science Division of the NASA Science Mission Directorate, NSF grant number AST-1238877, the University of Maryland, Eotvos Lorand University (ELTE), the Los Alamos National Laboratory and the Gordon and Betty Moore Foundation.

Author contributions

C.R.A. led the overall project and analysis, and wrote the majority of the paper; C.R.A. is also PI of the NOT and Gemini programmes used to collect data. V.F.B. performed the analysis to search for previous variability of the host galaxy, wrote text, made figure 4, and contributed to discussions regarding the link between the BH and host galaxy. B.M. performed the MOSFiT light curve analysis, made extended figure 3 and wrote text. R.J.F. reduced the HST data and observed for the Keck nights; R.J.F. is the PI of the Keck, Lick, and Hubble programmes used to collect data and wrote text, contributed to contributed to discussions regarding interpretation of the object and provided feedback on the manuscript. E.R.-R. contributed to discussions regarding the theoretical interpretation of the event. S.I.R. helped to perform the pPXF fitting of the host galaxy features and contributed to discussions. K.D.F. contributed to discussions regarding the nature of host galaxy and provided extensive feedback on manuscript drafts. K.A. triggered, reduced and analysed the Swift data used and contributed to discussions of the results and observations. K.D.F. also wrote text for the paper and provided comments on the manuscript. H.P. performed part the rate analysis of fast TDEs, contributed to discussions regarding the interpretation of the event and provided feedback on manuscript drafts. H.P. also performed vetting of candidates within the YSE survey. C.G. performed the spectral line profile analysis of the Hα emission, contributed to discussions and provided feedback on manuscript drafts. J.H. contributed to discussions and provided extensive feedback on manuscript drafts. M.R.D. contributed to discussions and performed the initial analysis regarding the rate of fast TDEs within YSE. K.D.A. triggered and reduced radio observations with the Very Large Array, and contributed to the interpretation of the resulting upper limits. G.D. reduced the GMOS spectra. T.H. reduced data, observed and submitted observing proposals for the event. D.O.J. reduced the YSE data for the event and performed PS1 operations for the survey. A.R. analysed and helped to interpret the forced YSE photometry of the event. M.R.S. reduced the LRIS and KAST spectra. K.T. provided manuscript comments and observed with Keck. G.T. observed and reduced the DEIMOS spectrum from Keck. C.M.C., L.D., N.E. and A.G. provided extensive feedback on the manuscript as a junior review panel. L.I., S.T., V.A.V. and Y.Z. also provided comments on the paper. N.A., C.C., N.K. and R.J.W. performed vetting of candidates within the YSE survey. D.A.C. wrote the collaboration software platform YSE-PZ and supported it and the server it runs on. T.J.L.d.B., K.C.C., C.C.L., E.A.M. and C.R-B. performed PS1 operations, including supporting the Pan-STARRS image processing pipeline that provided the initial astrometry and photometry. C.R.A., R.J.F., S.I.R., K.A., H.P., J.H., C.G., L.I., N.A., C.C. and R.W. all performed vetting of candidates within the YSE survey.

Competing interests

The authors declare no competing interests.

Additional information

Extended data is available for this paper at https://doi.org/10.1038/s41550-022-01811-y.

Supplementary information The online version contains supplementary material available at https://doi.org/10.1038/s41550-022-01811-y.

Correspondence and requests for materials should be addressed to C. R. Angus.

Peer review information *Nature Astronomy* thanks the anonymous reviewers for their contribution to the peer review of this work.

Reprints and permissions information is available at www.nature.com/reprints.

Publisher's note Springer Nature remains neutral with regard to jurisdictional claims in published maps and institutional affiliations.

Springer Nature or its licensor (e.g. a society or other partner) holds exclusive rights to this article under a publishing agreement with the author(s) or other rightsholder(s); author self-archiving of the accepted manuscript version of this article is solely governed by the terms of such publishing agreement and applicable law.

© The Author(s), under exclusive licence to Springer Nature Limited 2022

---

[1]DARK, Niels Bohr Institute, University of Copenhagen, Copenhagen, Denmark. [2]Department of Physics & Astronomy, Washington State University, Pullman, WA, USA. [3]Department of Astronomy and Astrophysics, University of California, Santa Cruz, CA, USA. [4]University of Southampton, Southampton, UK. [5]Department of Physics and Astronomy, University of California, Los Angeles, CA, USA. [6]Department of Astronomy, University of Illinois at Urbana-Champaign, Champaign, IL, USA. [7]Center for Astrophysical Surveys, National Center for Supercomputing Applications, Urbana, IL, USA. [8]OzGrav, School of Physics, The University of Melbourne, Parkville, Victoria, Australia. [9]ARC Centre of Excellence for All Sky Astrophysics in 3 Dimensions (ASTRO 3D), Melbourne, Victoria, Australia. [10]Department of Physics, The University of Hong Kong, Hong Kong, China. [11]David A. Dunlap Department of Astronomy and Astrophysics, University of Toronto, Toronto, Ontario, Canada. [12]The Observatories of the Carnegie Institute for Science, Pasadena, CA, USA. [13]Center for Interdisciplinary Exploration and Research in Astrophysics (CIERA) and Department of Physics and Astronomy, Northwestern University, Evanston, IL, USA. [14]School of Physics, Trinity College Dublin, The University of Dublin, Dublin, Ireland. [15]Department of Physics and Astronomy, The Johns Hopkins University, Baltimore, MD, USA. [16]Space Telescope Science Institute, Baltimore, MD, USA. [17]Las Cumbres Observatory, Goleta, CA, USA. [18]Department of Physics, University of California, Santa Barbara, Santa Barbara, CA, USA. [19]Department of Astronomy & Astrophysics, The Pennsylvania State University, University Park, PA, USA. [20]Institute for Computational & Data Sciences, The Pennsylvania State University, University Park, PA, USA. [21]Institute for Gravitation and the Cosmos, The Pennsylvania State University, University Park, PA, USA. [22]Institute for Astronomy, University of Hawaii, Honolulu, HI, USA.
✉e-mail: angus@nbi.ku.dk

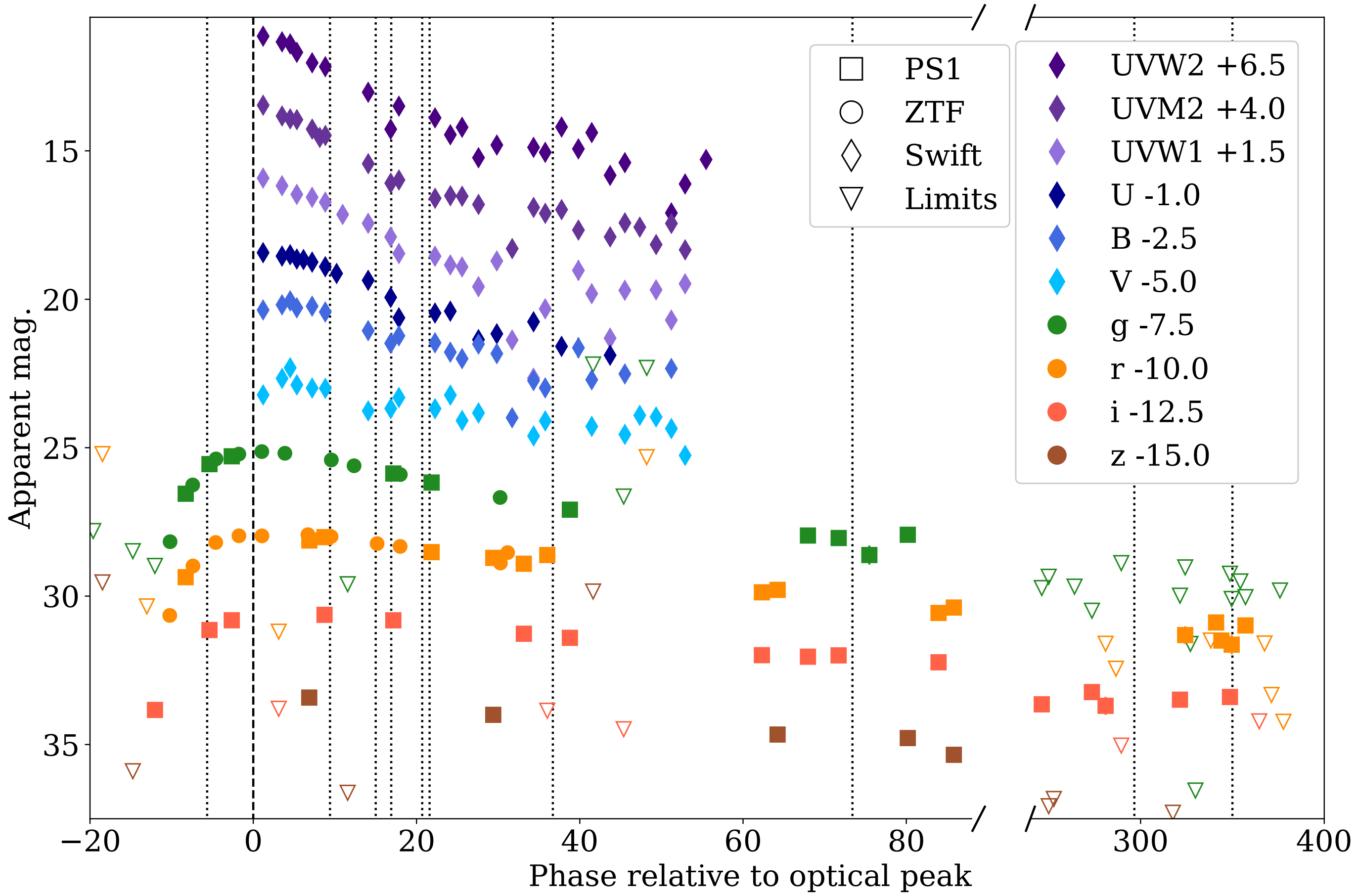

Extended Data Fig. 1 | Light curve of AT 2020neh. The UV-optical light curve of AT 2020neh throughout its observable lifetime. Grey dashed lines mark spectroscopic epochs, the dashed black line marks the peak of optical emission. Limits represent 3 σ upper limits to the flux for each telescope during periods of non-detection. There is an apparent gap in optical data between 40-60 days due to poor weather. AT 2020neh is first detected within YSE (PS1) imaging in the i-band, confirmed by with a g-band detection from ZTF <24 hours later. Pre-explosion monitoring allows for strong constraints to be placed upon the explosion epoch of the transient.

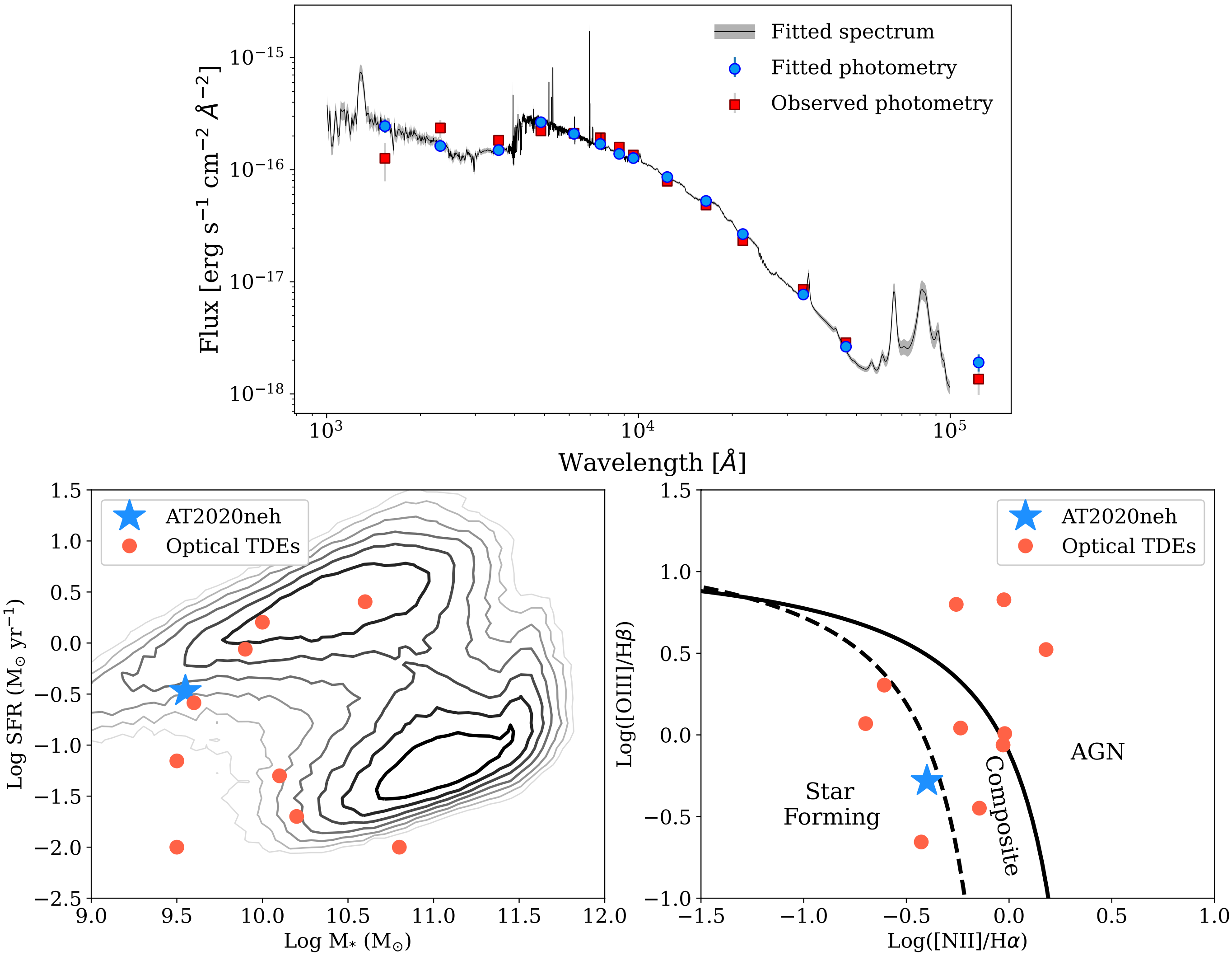

Extended Data Fig. 2 | Properties of the host of AT 2020neh. Top: The Prospector SED fit to the host galaxy photometry. All host photometry meaurements are shown with +/−1σ standard deviation uncertainties. Bottom left: Star formation rates vs. stellar masses for field galaxies (shown here is the SDSS spectroscopic sample as grey contours). The hosts of optical TDEs are shown in red (taken from 21). AT 2020neh sits comfortably within the parameter space occupied by other TDEs. Bottom right: A BPT diagram showing the regions where emission line ratios are indicative of ionisation from either an AGN, star formation or a composite of the two (78) The location of AT 2020neh is shown, alongside other optical TDE hosts with host SDSS spectra (21). The position of AT 2020neh inside of the star forming region of the diagram confirms the lack of an AGN component within the host.

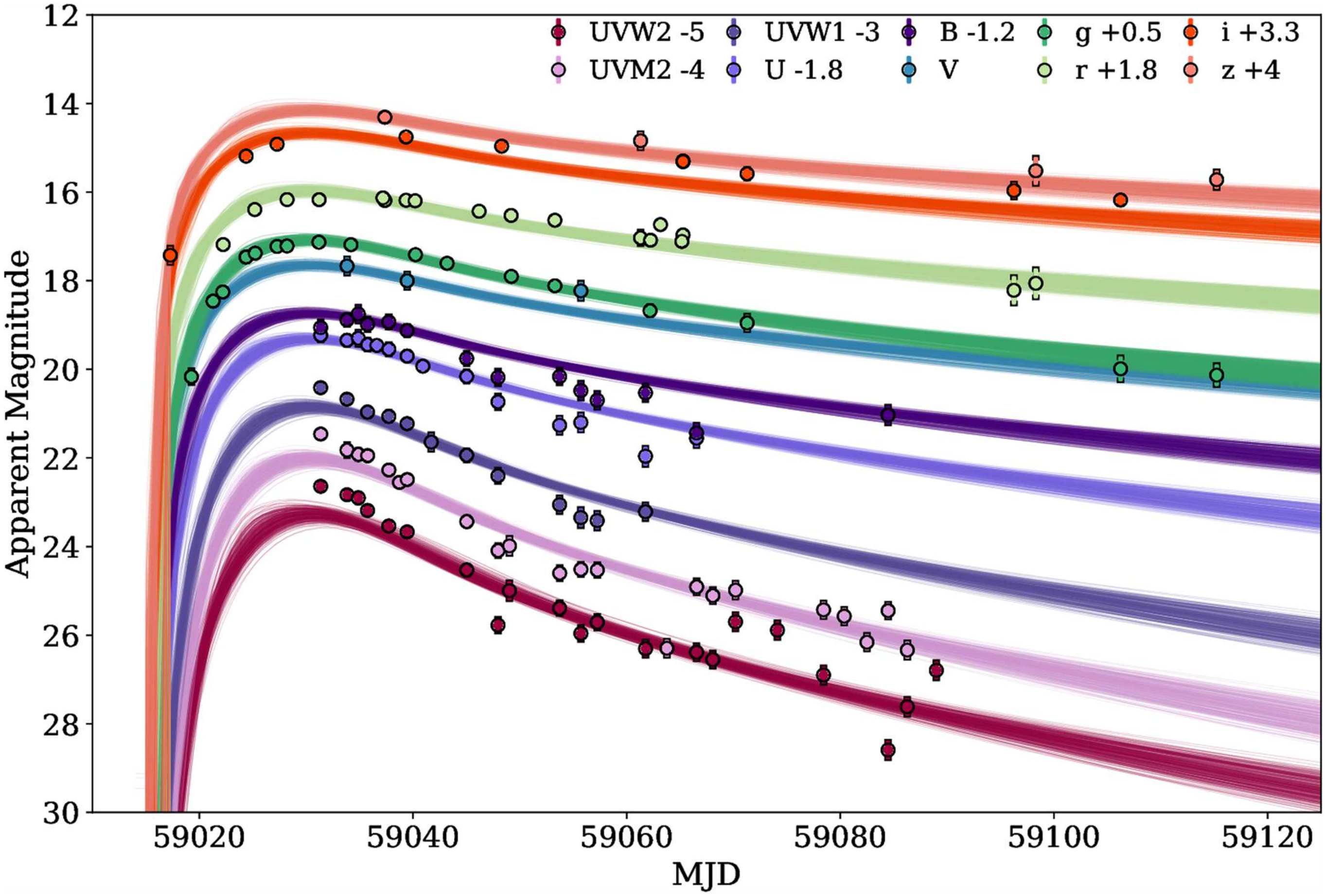

Extended Data Fig. 3 | MOSFiT modelling of the light curve of AT 2020neh. Photometry of AT 2020neh in UV-optical bands (offset for clarity) alongside all possible TDE light curves each constructed from the posterior parameter distribution. All photometric measurements are presented with +/−1 σ standard deviation uncertainties.